Cell Tissue Res (2012) 348:249–259
DOI 10.1007/s00441-011-1322-3

REGULAR ARTICLE

Histological and ultrastructural abnormalities in murine desmoglein 2-mutant hearts

Sebastian Kant · Philipp Krull · Sabine Eisner · Rudolf E. Leube · Claudia A. Krusche

Received: 15 December 2011 / Accepted: 16 December 2011 / Published online: 1 February 2012
© Springer-Verlag 2012

Abstract Mice carrying a deletion of the adhesive extracellular domain of the desmosomal cadherin desmoglein 2 develop an arrhythmogenic right ventricular cardiomyopathy-like phenotype with ventricular dilation, fibrosis and arrhythmia. To unravel the sequence of myocardial alterations and to identify potential pathomechanisms, histological analyses were performed on mutant hearts from the juvenile to the adult state, i.e., between 2 and 13 weeks. At an age of 2 weeks 30% of mutants presented lesions, which were visible as white plaques on the heart surface or in the septum. From 4 weeks onwards, all mutants displayed a cardiac phenotype. Dying cardiomyocytes with calcification were found in lesions of all ages. But lesions of young mutant animals contained high amounts of CD45+ immune cells and little collagen fibers, whereas lesions of the older animals were collagen-rich and harbored only a small but still significantly increased number of CD45+ cells. Electron microscopy further showed that distinct desmosomes cannot be distinguished in intercalated discs of mutant hearts. Widening of the intercellular cleft and even complete dissociation of intercalated discs were often observed close to lesions. Disturbed sarcomer structure, altered Z-discs, multiple autophagic vacuoles and swollen mitochondria were other prominent pathological features. Taken together, the following scenario is suggested: mutant desmoglein 2 cannot fully support the increased mechanical requirements placed on intercalated disc adhesion during postnatal heart development, resulting in compromised adhesion and cell stress. This induces cardiomyocyte death, aseptic inflammation and fibrotic replacement. The acute stage of scar formation is followed by permanent impairment of the cardiac function.

Keywords ARVC · Dilated cardiomyopathy · Aseptic inflammation · Transgenic mouse · Area composita

S. Kant · P. Krull · S. Eisner · R. E. Leube (✉) · C. A. Krusche (✉)
Institute of Molecular and Cellular Anatomy,
RWTH Aachen University,
Wendlingweg 2,
52074 Aachen, Germany
e-mail: rleube@ukaachen.de
e-mail: ckrusche@ukaachen.de

Introduction

Desmogleins (Dsgs) and desmocollins (Dscs) belong to the cadherin superfamily of calcium-dependent adhesion molecules and are localized to desmosomal cell-cell adhesion sites (Delva et al. 2009; Desai et al. 2009; Holthofer et al. 2007; Thomason et al. 2010). Their common molecular architecture is characterized by the four highly conserved extracellular domains EC1–EC4 that bridge the intercellular cleft. The EC domains are linked via a variable extracellular EA domain to the transmembrane segment. The intracellular cadherin-like sequence ICS has been identified as a common binding site for the linker molecule plakoglobin, whereas the other intracellular parts are cadherin type-specific. Plakoglobin—together with plakophilin and desmoplakin—mediate intermediate filament attachment. In humans, four desmoglein genes (DSG1, DSG2, DSG3, DSG4) and three desmocollin genes (DSC1, DSC2, DSC3) have been identified that are transcribed in cell type-specific combinations. The mouse genome contains two additional DSG1-related genes referred to as DSG5/DSG1β and DSG6/DSG1γ respectively (Holthofer et al. 2007).

The desmosomal cadherin isoforms Dsg2 and Dsc2 are the predominant desmosomal cadherins in heart (Holthofer et al. 2007). They localize to the intercalated disc, a prominent junctional complex, which mechanically and electrically couples cardiomyocytes to each other. The junctional subregions

supporting mechanical stability of intercalated discs are the fascia adhaerens, which serve as an anchor for actin filaments and desmosome-like structures, which anchor the desmin intermediate filament system (Franke et al. 2006). It has been recently demonstrated in mouse that both substructures mature postnatally into a highly integrated superstructure, the area composita (Franke et al. 2006; Pieperhoff and Franke 2007). As a consequence, Dsg2 and Dsc2 are distributed throughout the entire complex.

To examine the contribution of Dsg2-mediated adhesion to the cardiac function, we prepared mutant mice, in which the wild-type DSG2 alleles were replaced by mutant alleles coding for Dsg2 lacking parts of the adhesive EC1-EC2 domains (Krusche et al. 2011). Dilated ventricles and arrhythmias were observed in these animals. In addition, abundant fibrosis was noted, occurring either as fibrotic replacement in circumscribed regions or as diffuse interstitial fibrosis. Consequently, cardiac output was considerably reduced. Taken together, the animals present features of dilative cardiomyopathy (DCM) and arrhythmogenic right ventricular cardiomyopathy (ARVC) known to be caused by mutations in desmosomal proteins including also Dsg2 (Corrado et al. 2011; Fatkin and Graham 2002; Fressart et al. 2010; Posch et al. 2008; Richardson et al. 1996).

Our recent results led to the hypothesis that the DSG2 mutation induces myocardial infarction-like events, which occur as bursts and are followed by a healing process characterized by scar formation (Krusche et al. 2011). However, disease onset and progression as well as the cellular composition of the lesions over time remained unclear. The aim of this study was therefore to characterize the changes of cardiac tissue composition of DSG2 mutants during disease onset and progression in more detail. The observed fibrotic and immune cell response, as well as the detected structural alterations, are discussed with respect to the phenotypes described in ARVC and DCM patients, in the desmin null mouse (Mavroidis and Capetanaki 2002; Milner et al. 2000; Psarras et al. 2011) and the N271S-Dsg2 overexpressing transgenic mouse (Pilichou et al. 2009).

Material and methods

Animals

Mice were housed in the animal facility of the RWTH Aachen university clinic. They were fed a standard rodent lab diet (Ssniff, Soest, Gemany) and had free access to food and water. All experiments were performed in accordance with the guidelines for the care and use of laboratory animals. Litter mates were analyzed whenever possible. Due to the substantial intrauterine lethality of homozygous mutants, homozygous mutant males were mated with heterozygous females to increase mutant offspring. In this case, age-matched wild-type controls from parallel breedings had to be used. Mutant mice were backcrossed with the C57BL/6 J strain to reduce genetic variability.

Paraffin embedding and histology

The hearts of DSG2 mutant mice and wild-type controls were studied at an age of 2, 4, 6, 8 and 12 weeks. Hearts were fixed overnight in 4% buffered formaldehyde, dehydrated in a graded series of isopropanol and embedded in paraffin. Tissue sections 5 μm thick were stained with hematoxylin/eosin, von Kossa, or Heidenheim (azan). Tissue sections were photographed on an ApoTome.2 (Zeiss, Jena, Germany) using the Axiovision 4.83 software (Zeiss).

Electronmicroscopy

Hearts of 7- to 13-week-old animals (mutant mice $n=5$; wild-type mice $n=5$) were excised and directly dissected in fixative (4% formaldehyde/1% glutaraldehyde) (McDowell and Trump 1976). Regions containing scar tissue and myocardium devoid of macroscopically visible alterations (remote areas) were harvested separately. The samples were then minced into 1–2 mm^3 pieces, incubated for 2 h in fixative and 1 h in 1% OsO_4. Thereafter, the tissue was treated with 0.5% uranylacetate in 0.05 M sodium maleate buffer (pH 5.2) for 2 h in the dark. The tissue was dehydrated and embedded in araldite using acetone as intermedium. Polymerization was carried out at 60°C for 48 h. Ultrathin sections were prepared with a microtome. To enhance contrast, the sections were first treated with 3% uranyl acetate for 5 minutes and then with 0.08 M lead citrate solution for 4 minutes. Pictures were taken on an EM 10 (Zeiss) with a digital camera (Olympus, Münster, Germany) using the iTEM software (Olympus).

CD45 immunohistochemistry

Paraffin sections 5 μm thick were rehydrated and endogenous peroxidase was blocked by incubating the sections with 3% H_2O_2 in 70% ethanol. Sections were then pretreated with 100 mM EDTA (pH 8) for 45 minutes at room temperature to remove calcium deposits located in fibrotic lesions. Antigen retrieval was achieved by boiling sections in citrate buffer (10 mM; pH 6) for 3 minutes. Antibodies from hybridoma clone 30-F11 (rat monoclonal, BioLegend, Fell, Germany) were used to identify the CD45 antigen. Bound antibody was detected with the Histofine Simple Stain Mouse MAX PO rat kit (Medac, Wedel, Germany). DAB (Zytomed Systems, Berlin, Germany) was used as substrate to visualize the immunoreaction. Reactions were

documented with the help of an ApoTome.2 (Zeiss) using the Axiovision 4.83 software (Zeiss).

CD45 real-time RT-PCR

Total RNA was isolated with the PeqlabGold RNA kit (Peqlab, Erlangen, Germany). One μg of total RNA was reverse-transcribed into cDNA using the Transcriptor First Strand cDNA Synthesis Kit (Roche, Mannheim, Germany) with the oligo-$(dT)_{18}$ primer. Real-time PCR was performed with a Light Cycler and the Light Cycler TaqMan Master Kit (Roche). Forward and reverse primers (for, rev) and TaqMan probes (UPL) were selected with the help of the Universal Probe Library Assay Design Center (Roche). CD45 (Ptprc): for 5`cgggatgagacagttgatga 3`, rev 5` gtattctgcgcacttgttcct 3` and UPL#88. Housekeeping gene hydroxymethylbilane synthase (HMBS): for 5`tccctgaag gatgtgcctac3`, rev 5` aagggttttcccgtttgc 3` and UPL#79. The quantification of CD45 mRNA expression was done with the RelQuant Software (Roche) by normalizing the CD45 mRNA expression to the HMBS mRNA expression considering the efficiency of both PCRs.

Statistics

Measurements are given as mean±SEM. In case of comparing three different groups, the Kruskal–Wallis test and post hoc Dunn`s multiple comparison tests were used. When comparing two groups, the Mann–Whitney U test was applied. $P<0.05$ was considered as statistically significant.

Results

Calcification and fibrosis appear during early disease stages

Sixty percent of dissected mutant hearts did not reveal any obvious alterations upon visual inspection at 2 weeks after

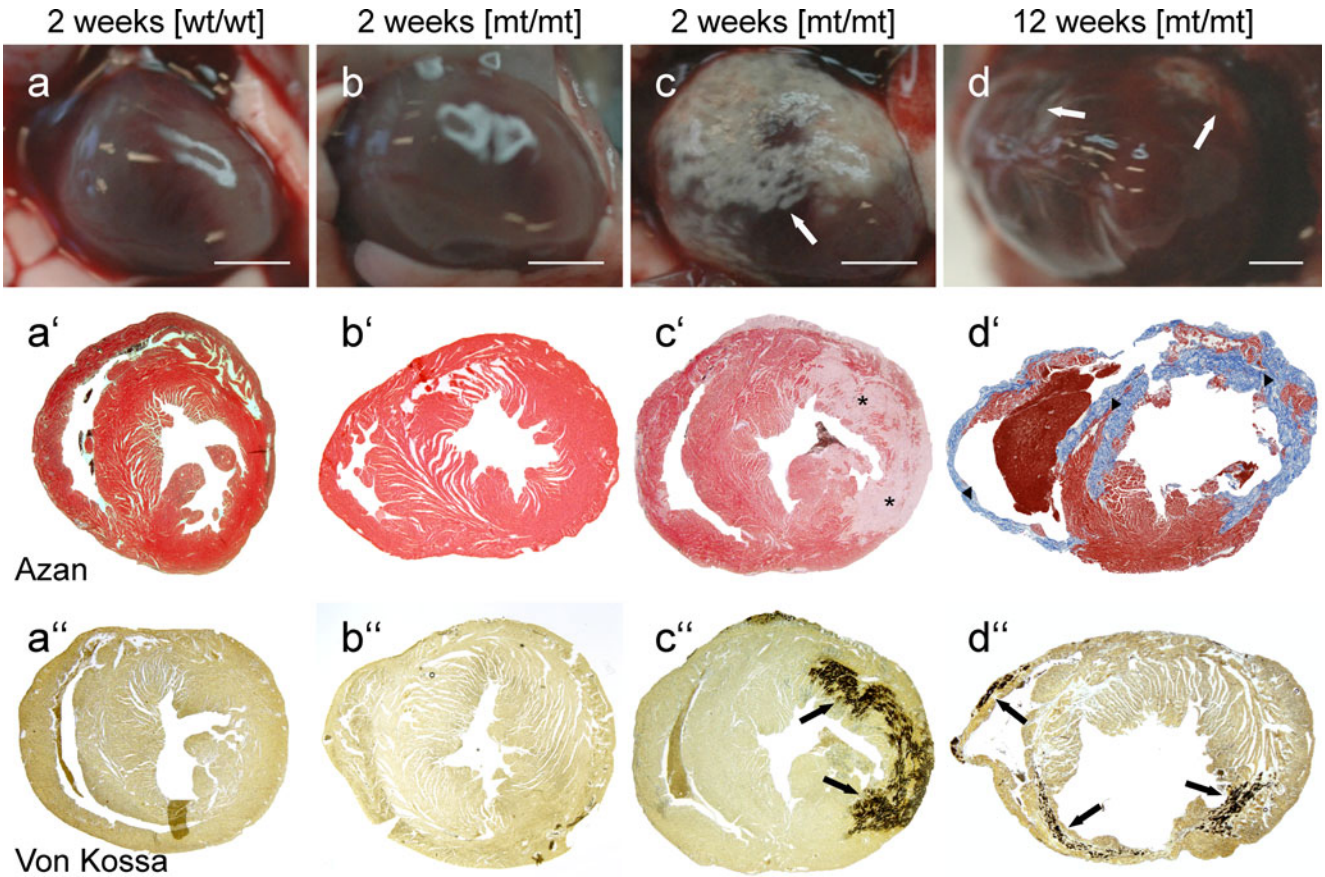

Fig. 1 Macroscopic (**a**, **b**, **c**, **d**) and microscopic appearance (azan stain in **a'**, **b'**, **c'**, **d'**; Kossa stain in **a"**, **b"**, **c"**, **d"**) of wild-type (*wt/wt*) and DSG2 mutant (*mt/mt*) hearts. Cardiac morphology and histology of most 2-week-old mutant mice (**b**–**b"**) are similar to that of the wildtype (**a**–**a"**). However, a few 2-week-old mutant mice show severe lesions that contain little collagen (**c**, *white arrow*) and present abundant calcification (**c"**, *black arrows*). At the age of 12 weeks, collagen-rich fibrotic lesions are readily apparent (**d'**, *arrowheads*) with residual calcification (**d"**, *black arrows*). *Scale bars* 1 mm (valid for each column)

birth (Fig. 1b, b', b"). In 30%, small white plaque-like cardiac lesions or slightly enlarged right ventricles were noted. These lesions were found all over the ventricular walls, including the free and septal walls of the right and left heart chambers. Most notably, extensive fibrotic lesions were seen in 10% of 2-week-old mutant hearts (Fig. 1c, c' and c"). These white plaque-like lesions covered substantial areas of the cardiac surface, including both ventricles (Fig. 1c). We have evidence that mice with such extensive lesions die before the fifth week (data not shown).

The macroscopically visible lesions corresponded to pale areas in azan-stained histological sections indicative of loss of red-appearing myofibril-rich cardiomyocytes (Fig. 1c'). It is noteworthy that these areas did not contain significant amounts of collagen fibers, which are blue in the azan stain. The black deposits identified by Kossa staining in such lesions further revealed calcification (Fig. 1c"). Degenerating and calcified cardiomyocytes were usually seen within these areas.

Examination of 12-week-old mutant hearts showed macroscopical and microscopical alterations in all instances (Fig. 1d). The hearts were enlarged and presented fibrotic lesions. In general, these lesions appeared to be more scar-like than those in younger animals, as they contained extensive collagen deposits and fewer cells (Fig.1d'). Calcinosis was also frequent but appeared to be more restricted in comparison to that observed in the collagen-free lesions of younger animals (compare Fig. 1d" with Fig. 1c").

Hearts from 2-, 4- and 6-week-old DSG2 mutants were studied next to further define the sequential nature and the onset of the disease process. From 4 weeks onward, all DSG2 mutants displayed cardiac lesions (Fig. 2). At this stage, lesions with varying degrees of collagen deposits were seen (Fig. 2b, b'), whereas in 6-week-old mutants all lesions showed extensive collagen deposition (Fig. 2c, c'). Degenerated, calcified cardiomyocytes were usually detected within the scars of mutant mice at 2, 4 and 6 weeks (Fig. 2a", b", c"). Taken together, the observations suggest that fully differentiated scar tissue develops as a substitute for the lost cardiomyocytes between 2 and 6 weeks.

Invasion of CD45-positive cells is linked to lesion formation

Since cardiomyocyte death has been shown to induce immune cell infiltration (Frantz et al. 2009), we searched for the presence of immune cells in mutant hearts. Accumulations of round cells were already obvious in azan-stained sections (Fig. 2a'). To demonstrate that they contain immune cells, immunohistochemisty was performed detecting the general leukocyte marker CD45 antigen (Fig. 3). Large amounts of CD45+ immune cells were detected in hearts of 2-week-old DSG2 mutant mice with fibrotic lesions

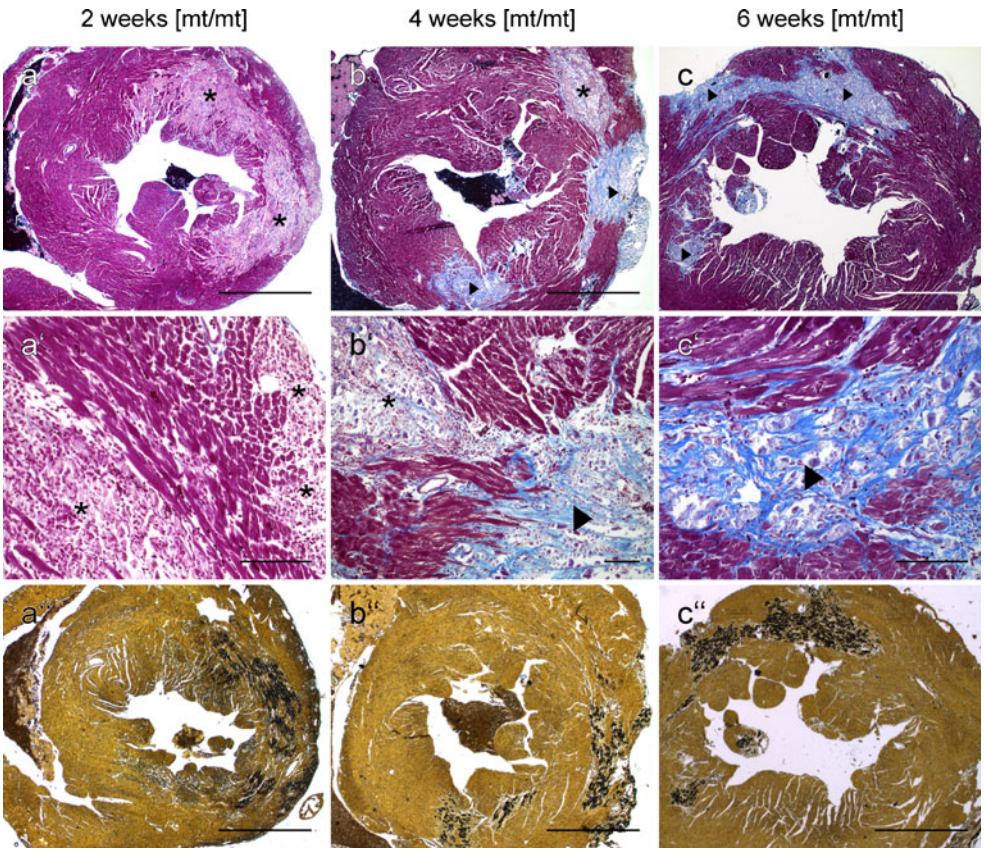

Fig. 2 Histology of myocardial lesions in 2–6 week old DSG2 mutants (*mt/mt*). Azan stains are shown at low and high magnification in **a**–**c** and **a'**–**c'** respectively. Corresponding Kossa stains are presented in **a"**–**c"**. Note that the lesions in 2-week-old DSG2 mutant hearts are cell-rich (**a'**, **a"**; *stars*) and contain calcifications (**a"**). In contrast, lesions of 6-week-old mutants show increasing amounts of collagen-rich extracellular matrix (**c**, **c'**, *arrowheads*) and some calcified cardiomyocytes (**c"**). In 4-week-old mutants, lesions with different amounts of collagen deposition are found (**b**, **b'**): a lesion with low collagen content (*star*) is next to a lesion with high collagen content (*arrowhead*). *Scale bars* 1 mm in **a**–**c** and **a"**–**c"**; 100 μm in **a'**–**c'**

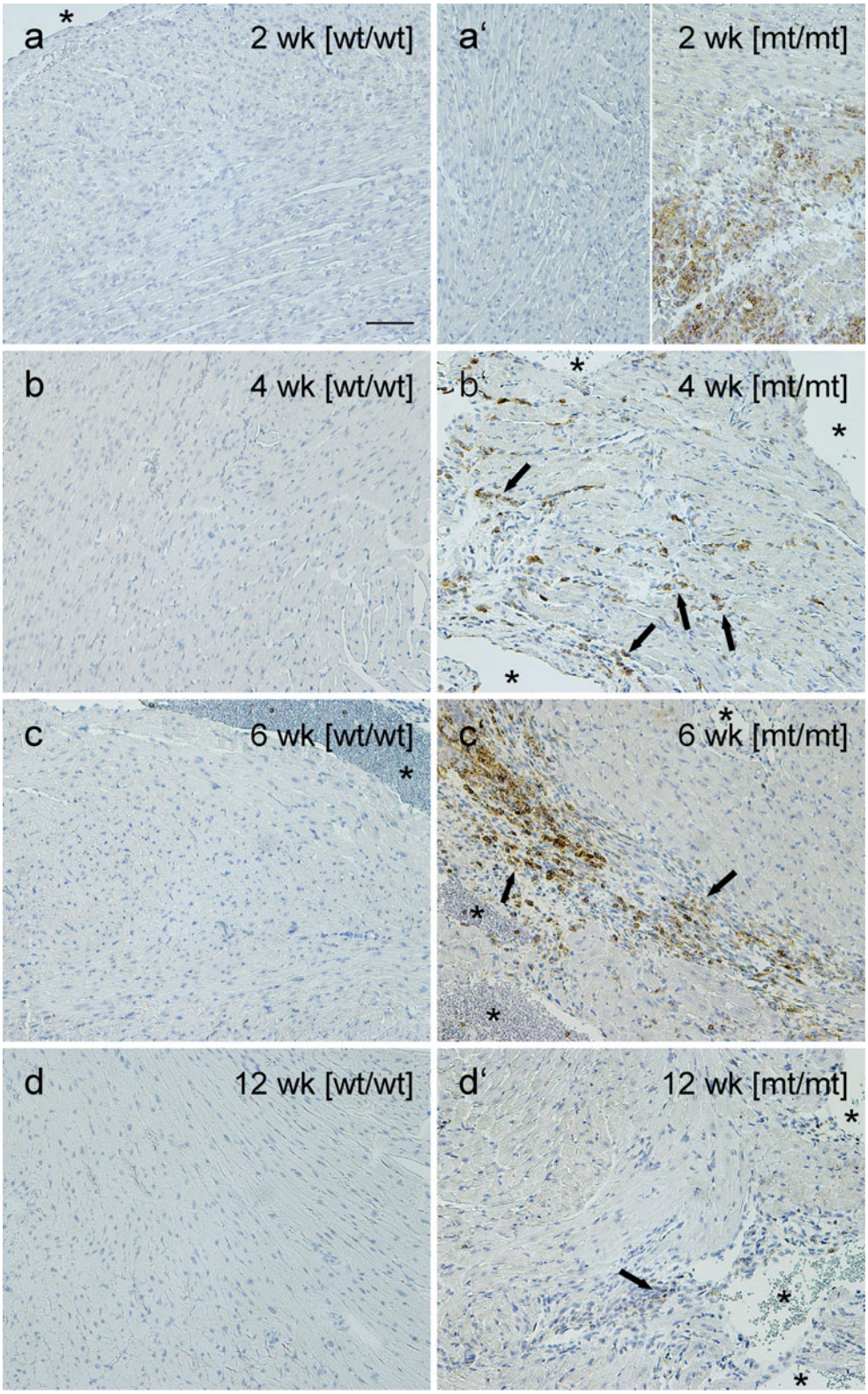

Fig. 3 CD45 immunohistology of wild-type (*wt/wt*; **a**–**d**) and DSG2 mutant hearts (*mt/mt*; **a'**–**d'**). Note that 2-week-old (*2 wk*) mice without lesions are devoid of CD45+ immune cells, as is the case in the wildtype (**a**, *left panel* in **a'**), whereas 2-week-old mice with lesions show extensive invasion of CD45+immune cells (**a'**, *right panel*). CD45 staining remains elevated in 4- and 6-week-old mutants (*4 wk*, *6 wk*; *black arrows* in *b'*, *c'*), i.e., during lesional remodeling. Only few immune cells remain in the scar tissue of 12-week-old mutants (*12 wk*; *black arrow* in **d'**). *Stars* mark vascular or ventricular lumina. *Scale bar* 100 μm (same magnification for all images)

(Fig. 3a', right part). In contrast, CD45+ immune cells were rarely found in wild-type littermates and in 2-week-old mutants without cardiac lesions (Fig. 3a, a' left part, b, c, d). The presence of these cells persisted in 4- and 6-week-old mutants, albeit at a lower level but still considerably more than in wild-type mice of the same age (Fig. 3b, b', c, c'). The CD45+ immune cells were primarily localized in the large scar-like lesions but were also present in areas with increased interstitial fibrosis (Fig. 3b'). In intact-appearing myocardium of mutants only single CD45+ immune cells

were observed at all time points (Fig. 3a' left part, b', c', d') as is the case in the wild type (Fig. 3a, b, c, d). The number of CD45+ immune cells in fibrotic lesions further decreased in older animals (12 weeks in Fig. 3d'). This is best appreciated comparing Fig. 3a' left part, b', c' and Fig. 3d'. This phenomenon correlates with the gradual decrease of lesional calcification and reduction of necrotic cardiomyocytes (see above).

Real-time RT-PCR was performed to quantitatively assess the level of CD45 mRNA expression (Fig. 4). The CD45 mRNA levels did not differ between wild-type and lesion-free mutant hearts at 2 weeks (0.28±0.07 and 0.37± 0.04 arbitrary units respectively; Fig. 4a). In contrast, CD45 mRNA expression was 9.6 times higher in 2-week-old mutants with cardiac lesions than in wild-type controls (2.69±1.08 arbitrary units vs 0.28±0.07, Kruskal–Wallis test: p=0.0349). At the age of 8 and 12 weeks, the CD45 mRNA expression was still elevated in mutant mice by a factor of 3.3 and 2.1 respectively (Fig. 4b, c). The differences are statistically significant (8 weeks: 0.61±0.08 vs 2.03±0.46 arbitrary units; Mann–Whitney test: p=0.0159; 12 weeks: 0.36±0.05 vs 0.74±0.08 arbitrary units, Mann–Whitney test: p=0.0159). Taken together, CD45 mRNA expression peaks at time points when cardiomyocytes die and fibrotic repair is initiated. Then, the expression declines gradually with age and scar maturation.

Changes of intercalated disc morphology imply compromised adhesion in DSG2 mutant mice

To identify ultrastructural alterations, transmission electron microscopy was performed on hearts obtained between 7 and 13 weeks of age. The initial focus was on intercalated disc morphology. In the wild type, typical desmosome-like areas with prominent electron-dense plaques were readily distinguishable between the actin-anchoring fasciae adhaerentes (arrows in Fig. 5a). In contrast, mutants presented a much more homogenous intercalated disc region and individual desmosomal-like plaques could not be distinguished (Fig. 5b, Fig. 6a). In addition, widening of the intercellular cleft was frequently observed but difficult to quantify given the slightly different sectional angles (compare, for example, Fig. 5b and Fig. 6a, b with Fig. 5a). Most notably, however, partial and even complete dissociation of cardiomyocytes at the intercalated disc area was often seen (Fig. 5c, Fig. 6c and Fig. 7a, b). These disconnected cardiomyocytes were mostly detected close to fibrotic lesions.

Furthermore, sarcomer structure was often disturbed in mutant mice, as evidenced by disordered Z-discs with bright halos and irregular filament alignment (Fig. 5d, Fig. 7a). Complete sarcomer disruption was noted in some cardiomyocytes of mutant mice (Fig. 7b).

Mitochondrial abnormalities were other common features of mutant cardiomyocytes (Fig. 5c and 6a). The mitochondria were swollen and had disrupted cristae. Additional signs of compromised cell function were the multiple autophagic vacuoles in mutant hearts. They often had a multilamellar interior. Their presence can be taken as an indication of enhanced organelle turnover, presumably also including the damaged mitochondria (Fig. 5c and 6b). In addition, lipid droplets were detected more frequently in mutant than in wild-type hearts (Fig. 6c).

Cardiomyocytes disintegrate, die and are replaced by fibrotic scar tissue

Fibrotic lesions were readily identified by their presence of extensive extracellular matrix with bundles of collagen fibers in between typical fibroblasts (Fig. 7c, d). Remnants of cardiomyocytes were seen within such lesions. They were often surrounded by a rim of calcification (Fig. 7d). Calcium deposits were also frequently observed in association with collagen fibers (Fig. 7c). Macrophages were detected within lesions (Fig. 7d). They contain vacuoles with cellular material, which is most likely derived from dying cardiomyocytes. This is in accordance with our immunohistological findings.

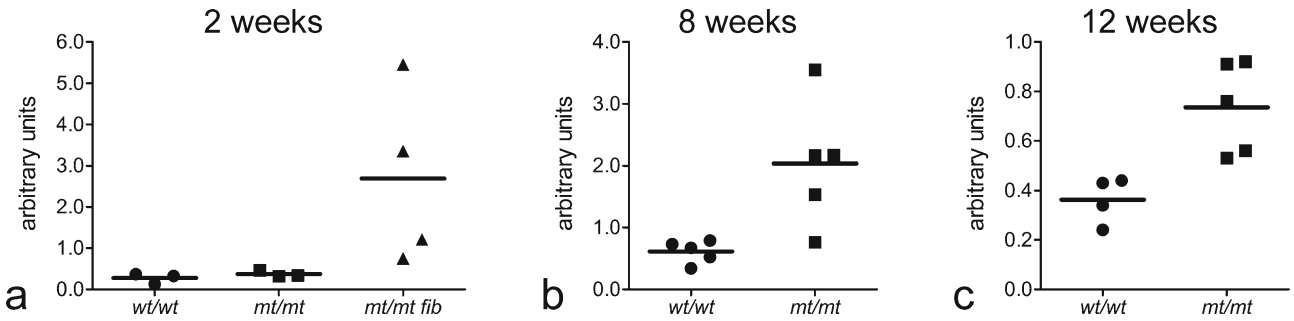

Fig. 4 Results of CD45 real-time RT-PCR analyses. CD45 mRNA expression was determined by real-time RT-PCR in wild-type (*wt/wt*) and mutant (*mt/mt*) hearts at different ages. Note that at 2 weeks CD45 expression is only increased in DSG2 mutant mice with myocardial lesions (**a**; *mt/mt fib*; Kruskal–Wallis test: p=0.0349), whereas those without an overt phenotype do not differ from the wildtype (**a**). At 8 and 12 weeks, all DSG2 mutant mice display a cardiac phenotype and CD45 mRNA expression levels are significantly elevated (**b**, **c**; Mann–Whitney test: p=0.0159 each)

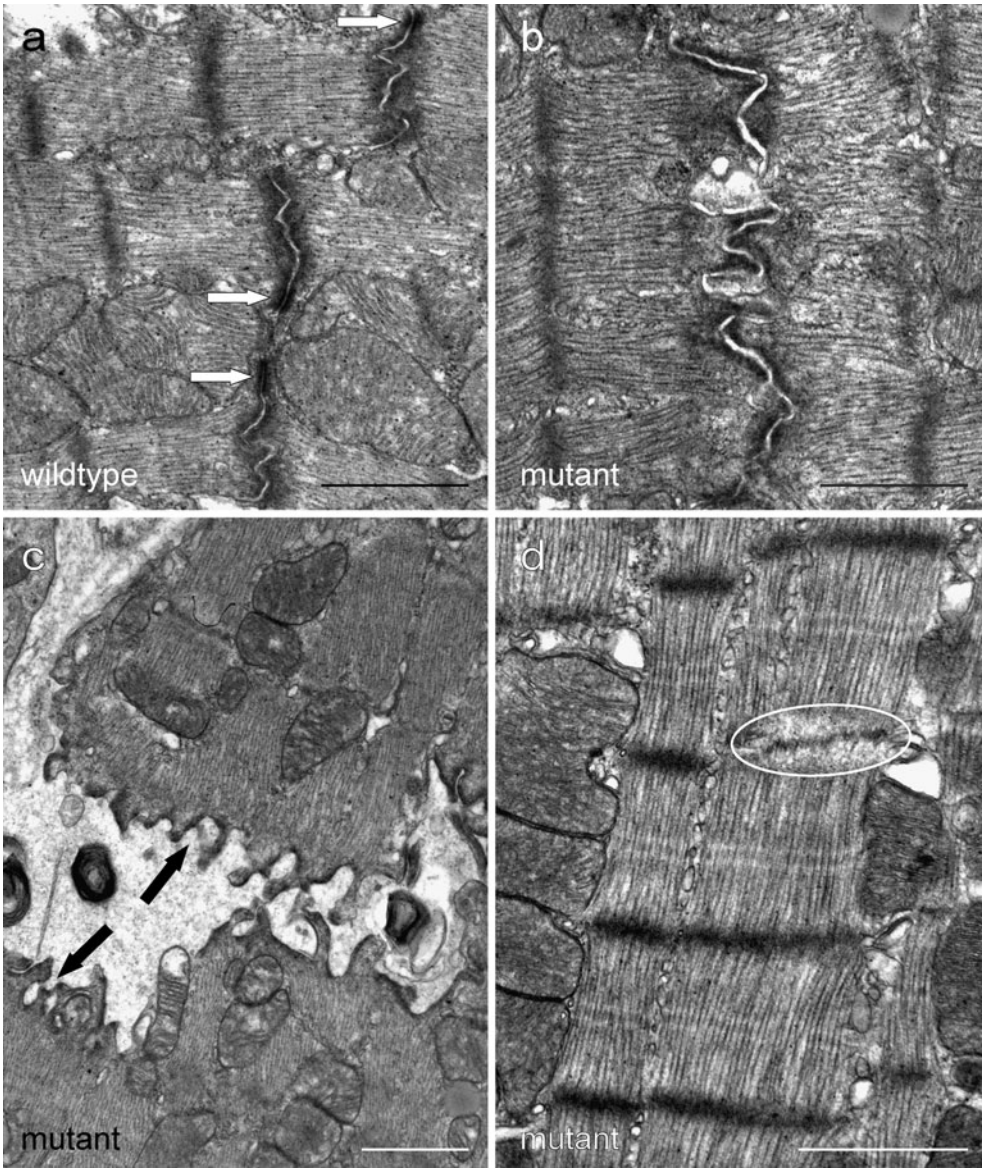

Fig. 5 Electron microscopy of heart tissue from wild-type and DSG2 mutant hearts. Note the distinct desmosome-like structures in the wildtype (**a**; *white arrows*) that are lacking in the mutant (**b**). In addition, complete intercalated disc rupture is seen in mutant hearts (**c**; *black arrows*). Abnormal Z-disc structure is also encountered in the mutant (**d**; *oval*). *Scale bars* 1 μm

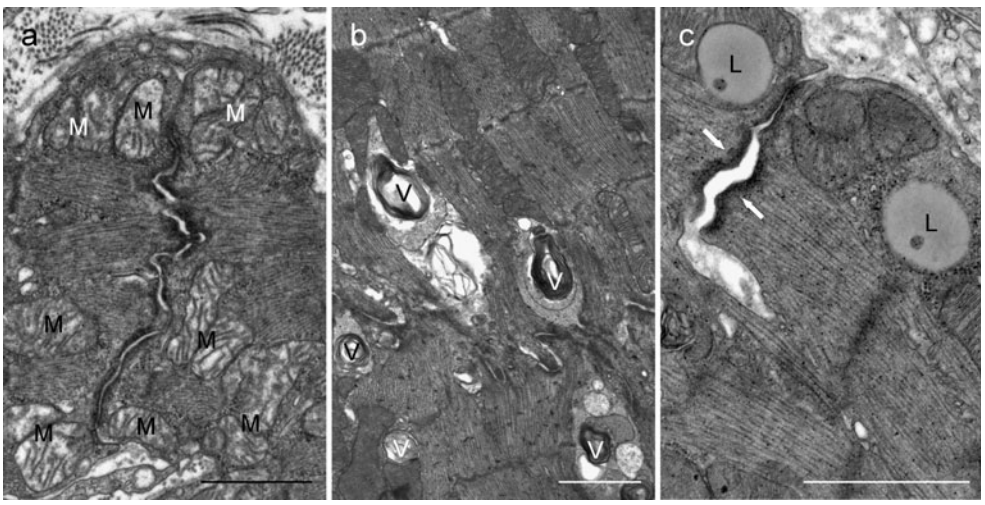

Fig. 6 Electron microscopy of ultrastructural changes in DSG2 mutant hearts. Swollen and partially disrupted mitochondria (*M*, **a**) are frequently seen in mutant hearts. Multiple autophagic vacuoles (*V*, **b**) are also often detectable and occasional lipid droplets are present (*L*, **c**). Note the disrupted intercalated disc in **c** (*white arrows*). *Scale bars* 1 μm

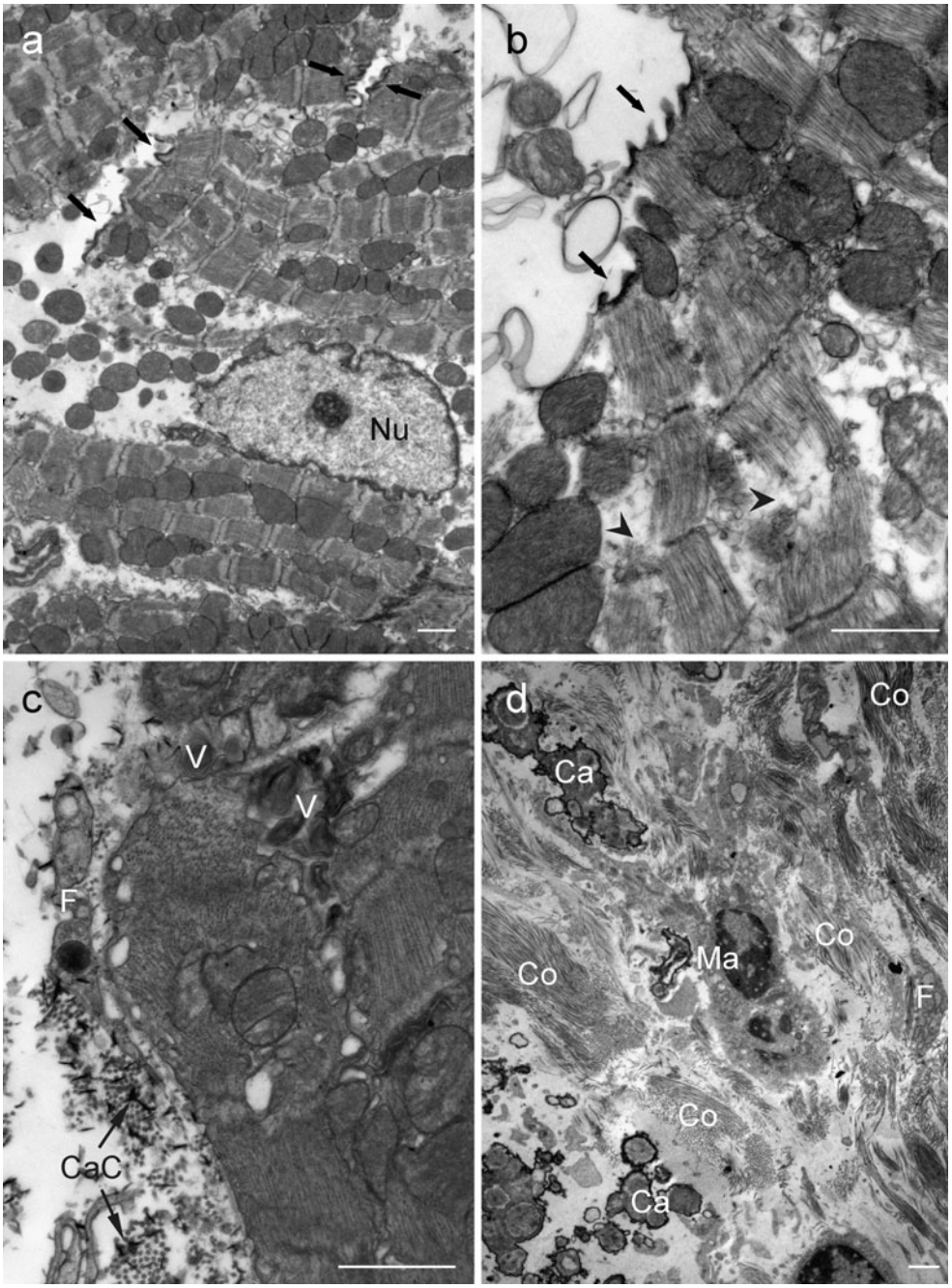

Fig. 7 Electron microscopy of fibrotic scars and their adjacent zones in DSG2 mutant hearts at late stages of disease development. Cardiomyocytes with disrupted intercalated discs are frequently encountered close to or within fibrotic lesions (**a**, **b**; *black arrows*). In addition, completely ruptured sarcomers are found within cardiomyocytes (**b**; *arrowheads*). Calcification of the extracellular matrix (**c**; *CaC*; *F*, fibroblast) and rims of calcification surrounding remnants of cardiomyocytes (**d**; *Ca*) are often present in fibrotic regions containing collagen fibers (*Co*) and fibroblasts (*F*). In addition, single macrophages (**d**; *Ma*) are detectable in fibrotic lesions. The occurrence of autophagic vacuoles (**c**; *V*) indicates cellular stress and organelle removal. *Scale bars* 1 μm

So far we have not seen cardiomyocyte nuclei presenting typical signs of necrosis and/or apoptosis (Fig. 7a).

Discussion

The examination of hearts from DSG2 mutant mice between 2 and 13 weeks implies that the mutant Dsg2 protein initiates a distinct sequence of pathological events resulting in ventricle dilatation and loss of cardiac function. The deletion of exons 4-6 of the DSG2 gene leads to the production of a Dsg2 lacking major parts of the extracellular EC1/EC2 domains. Since these domains are implicated in trans-interactions of desmosomal cadherins (Holthofer et al. 2007; Huber 2003), the mutant Dsg2 protein is probably less adhesive than its wild-type counterpart. Furthermore, the mutant protein may lead to disturbance of the highly organized array of cadherins within the junction (Al-Amoudi et al. 2007). Since Dsg2 is not only located in desmosome-like structures but also in the fasciae adhaerentes of intercalated discs from the third week after birth onwards (Pieperhoff and Franke 2007), both junctions are probably affected by the mutation. At the ultrastructural level a loss of desmosome-like structures within the

intercalated discs was seen in mutant hearts, a feature also described for the myocardium of ARVC patients (Basso et al. 2006). Furthermore, in adult DSG2 mutant mice a detachment of neighboring cardiomyocytes was observed primarily along intercalated discs, indicating impairment of intercellular contacts primarily at this special site. Whether the observed cardiomyocyte detachment at the intercalated disc is solely a mechanical problem and/or is a consequence of impaired signaling (Berkowitz et al. 2008; Hirschy et al. 2010; Lanza et al. 2008) needs further investigation.

Newborn, apparently healthy mutants are obviously able to compensate for the dysfunction of the mutant Dsg2 for some time. The previously reported increase in mRNA expression of the cardiac stress marker ANF in a subset of 2-week-old and lesion-free mutants, however, suggests that the hearts are already under mechanical stress even in the absence of clear morphological alterations (Krusche et al. 2011 and unpublished data).

The myocardium decompensates and develops macroscopical lesions in mutant mice between 2-4 weeks. It is of importance to note that desmin null mice (Mavroidis and Capetanaki 2002) and mice overexpressing mutant N271S-Dsg2 (Pilichou et al. 2009) show a similar profile of disease onset. The reason for the apparent myocardial vulnerability during this time period is not known but postnatal development and maturation of the heart may be determining factors. During the first 4 weeks of life, corresponding roughly to the first 10 years of human life, cardiac changes take place that affect cardiac function and workload (Xu et al. 2005). The heart adapts to the rapidly increasing body weight, first by hyperplasia then by hypertrophy (Leu et al. 2001). At the same time, the heart rate increases from 180 beats/minute to 450 beats/minute (Zhou et al. 2003). In parallel, the composition of sarcomeric proteins and ion channels changes (Harrell et al. 2007; Morkin 2000), intercalated disc proteins are rearranged to establish the mixed area composita (Pieperhoff and Franke 2007) and there is a shift in substrate usage for ATP generation (Lehman and Kelly 2002). At the age of 2 weeks, mice also start to become physically more active, which increases cardiac workload and coincides with disease onset in mutant mice.

The acute phase of disease manifestation is characterized by the appearance of cell-rich lesions, which contain some calcified and dying cardiomyocytes. A high proportion of cells within these lesions are CD45+ immune cells, indicating an aseptic inflammatory reaction. It will be of interest to find out whether this reaction is initiated by DAMPs (danger-associated molecular patterns) (Matzinger 1994) released from dying cardiomyocytes (Arslan et al. 2011). Such inflammatory infiltrates have also been described in desmin null mice (Psarras et al. 2011) and the transgenic N271S-Dsg2 mouse (Pilichou et al. 2009).

The histological data from our 4- to 8-week-old mutants imply that a cardiac repair process is initiated after the acute phase of disease onset. This process is characterized by removal of dead cardiomyocytes via macrophages and their replacement by connective tissue and extracellular matrix. The initial fulminant immune cell infiltration slowly decreases with increasing age. It will be interesting to find out which immune cell subtypes are present in the lesions and whether immune cell subsets change over time, as reported for myocardial infarction and subsequent healing (Nahrendorf et al. 2007).

Fresh lesions could not be detected in any of the 8- and 12-week-old mutants. Instead, the lesions resemble scar tissue and are composed of extracellular matrix, fibroblasts, and remnants of calcified, necrotic cardiomyocytes. In the diseased myocardium, focal accumulation of CD45+ immune cells were also detected. These foci were found close to or within fibrous scar tissue containing necrotic cardiomyocytes. Such patchy inflammatory infiltrates are also present in hearts of human ARVC patients (Asimaki and Saffitz 2011; Basso et al. 1996; Corrado et al. 2011). Furthermore, sustained presence of immune cells was also noted in desmin null mice (Psarras et al. 2011). These accumulations can be taken as indicators of local cardiomyocyte stress and/or death reflecting chronic disease progression, albeit at a slower speed than in young mutant animals. We hypothesize that the adult myocardium does not possess the acute vulnerability of the developing myocardium. But it has to be kept in mind that the mutant heart has to cope with the continued mechanical stress and the additional stress imposed by the dysfunctional fibrous

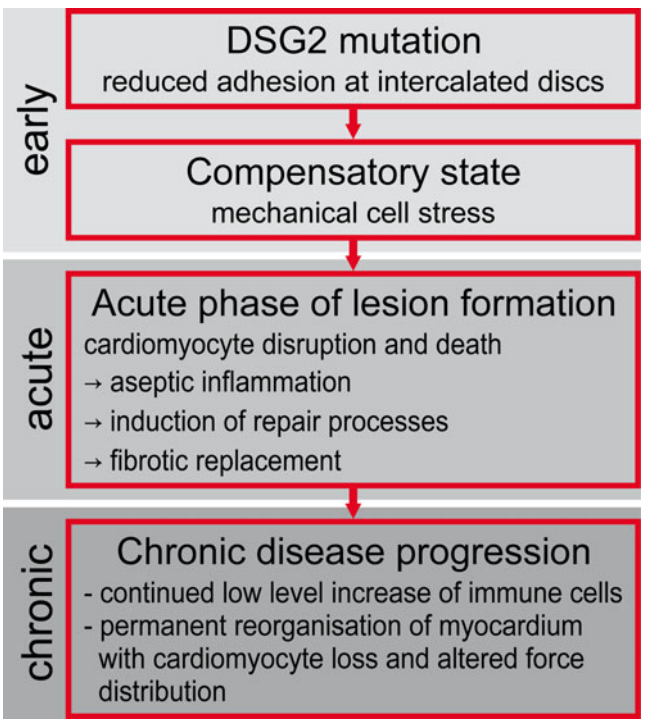

Fig. 8 Hypothetical model of disease induction and progression caused by the DSG2 mutation. For further details see Discussion

tissue replacement. Consequently, cardiomyocytes close to diseased areas showed ultrastructural abnormalities such as disrupted sarcomers and damaged mitochondria, indicating circumscribed tissue remodeling. Another indicator of continued myocardial stress and remodeling in the adult DSG2 mutants is the increased number of autophagic vacuoles. Autophagy is involved in the degradation of cell organelles and sarcomers. It is enhanced during pathological cardiac stress, in myocardial infarction, in cardiomyopathies and heart failure (Christians and Benjamin 2011; Nakai et al. 2007; Nishida et al. 2009). Consequently, autophagy may serve as an adaptive response supporting survival and function of the stressed cardiomyocytes (Nakai et al. 2007). However, autophagy is also detected in the context of cardiac cell death (Portbury et al. 2011; Whelan et al. 2010).

Fig. 8 summarizes our current hypotheses on the pathogenesis of DSG2-related cardiomyopathy in the mouse model. Compromised Dsg2 adhesion at intercalated discs initiates the disease process during postnatal cardiac development, i.e., between 2 and 4 weeks after birth, when compensatory mechanisms become insufficient to cope with the increased mechanical stress. An acute, infarct-like damage is inflicted on the myocardium. The intercalated discs rupture and cardiomyocytes die. The acute damage of the myocardium induces cardiac repair processes characterized by aseptic inflammation and subsequent fibrosis. The ensuing chronic phase of disease progression is much slower and occurs from 8 weeks onward. It is characterized by a continued moderate increase of immune cells and slow cardiomyocyte loss, eventually leading to live-threatening arrhythmias and heart failure because of altered force distribution. Many of these features are shared by human ARVC patients who either die early from sudden death during physical exertion or present protracted disease progression with much longer life expectancy (Bauce et al. 2011; Judge 2011).

Acknowledgements We are grateful for the expert technical assistance of Marina Lürkens-Weber. This work was supported by the German Research Council (LE 566/11-1) and a grant from the IZKF of Aachen University.

References

Al-Amoudi A, Diez DC, Betts MJ, Frangakis AS (2007) The molecular architecture of cadherins in native epidermal desmosomes. Nature 450:832–837

Arslan F, de Kleijn DP, Pasterkamp G (2011) Innate immune signaling in cardiac ischemia. Nat Rev Cardiol 8:292–300

Asimaki A, Saffitz JE (2011) The role of endomyocardial biopsy in ARVC: looking beyond histology in search of new diagnostic markers. J Cardiovasc Electrophysiol 22:111–117

Basso C, Thiene G, Corrado D, Angelini A, Nava A, Valente M (1996) Arrhythmogenic right ventricular cardiomyopathy. Dysplasia, dystrophy, or myocarditis? Circulation 94:983–991

Basso C, Czarnowska E, Della Barbera M, Bauce B, Beffagna G, Wlodarska EK, Pilichou K, Ramondo A, Lorenzon A, Wozniek O, Corrado D, Daliento L, Danieli GA, Valente M, Nava A, Thiene G, Rampazzo A (2006) Ultrastructural evidence of intercalated disc remodelling in arrhythmogenic right ventricular cardiomyopathy: an electron microscopy investigation on endomyocardial biopsies. Eur Heart J 27:1847–1854

Bauce B, Rampazzo A, Basso C, Mazzotti E, Rigato I, Steriotis A, Beffagna G, Lorenzon A, De Bortoli M, Pilichou K, Marra MP, Corbetti F, Daliento L, Iliceto S, Corrado D, Thiene G, Nava A (2011) Clinical phenotype and diagnosis of arrhythmogenic right ventricular cardiomyopathy in pediatric patients carrying desmosomal gene mutations. Heart Rhythm 8:1686–1695

Berkowitz P, Chua M, Liu Z, Diaz LA, Rubenstein DS (2008) Autoantibodies in the autoimmune disease pemphigus foliaceus induce blistering via p38 mitogen-activated protein kinase-dependent signaling in the skin. Am J Pathol 173:1628–1636

Christians ES, Benjamin IJ (2012) Proteostasis and REDOX state in the heart. Am J Physiol Heart Circ Physiol 301(1):H24–H37

Corrado D, Basso C, Pilichou K, Thiene G (2011) Molecular biology and clinical management of arrhythmogenic right ventricular cardiomyopathy/dysplasia. Heart 97:530–539

Delva E, Tucker DK, Kowalczyk AP (2009) The desmosome. Cold Spring Harb Perspect Biol 1:a002543

Desai BV, Harmon RM, Green KJ (2009) Desmosomes at a glance. J Cell Sci 122:4401–4407

Fatkin D, Graham RM (2002) Molecular mechanisms of inherited cardiomyopathies. Physiol Rev 82:945–980

Franke WW, Borrmann CM, Grund C, Pieperhoff S (2006) The area composita of adhering junctions connecting heart muscle cells of vertebrates. I. Molecular definition in intercalated disks of cardiomyocytes by immunoelectron microscopy of desmosomal proteins. Eur J Cell Biol 85:69–82

Frantz S, Bauersachs J, Ertl G (2009) Post-infarct remodelling: contribution of wound healing and inflammation. Cardiovasc Res 81:474–481

Fressart V, Duthoit G, Donal E, Probst V, Deharo JC, Chevalier P, Klug D, Dubourg O, Delacretaz E, Cosnay P, Scanu P, Extramiana F, Keller D, Hidden-Lucet F, Simon F, Bessirard V, Roux-Buisson N, Hebert JL, Azarine A, Casset-Senon D, Rouzet F, Lecarpentier Y, Fontaine G, Coirault C, Frank R, Hainque B, Charron P (2010) Desmosomal gene analysis in arrhythmogenic right ventricular dysplasia/cardiomyopathy: spectrum of mutations and clinical impact in practice. Europace 12:861–868

Harrell MD, Harbi S, Hoffman JF, Zavadil J, Coetzee WA (2007) Large-scale analysis of ion channel gene expression in the mouse heart during perinatal development. Physiol Genomics 28:273–283

Hirschy A, Croquelois A, Perriard E, Schoenauer R, Agarkova I, Hoerstrup SP, Taketo MM, Pedrazzini T, Perriard JC, Ehler E (2010) Stabilised beta-catenin in postnatal ventricular myocardium leads to dilated cardiomyopathy and premature death. Basic Res Cardiol 105:597–608

Holthofer B, Windoffer R, Troyanovsky S, Leube RE (2007) Structure and function of desmosomes. Int Rev Cytol 264:65–163

Huber O (2003) Structure and function of desmosomal proteins and their role in development and disease. Cell Mol Life Sci 60:1872–1890

Judge DP (2011) Cardiovascular genetics provides new insights for early onset arrhythmogenic right ventricular dysplasia/cardiomyopathy. Heart Rhythm 8:1696–1697

Krusche CA, Holthofer B, Hofe V, van de Sandt AM, Eshkind L, Bockamp E, Merx MW, Kant S, Windoffer R, Leube RE (2011) Desmoglein 2 mutant mice develop cardiac fibrosis and dilation. Basic Res Cardiol 106:617–633

Lanza A, Cirillo N, Rossiello R, Rienzo M, Cutillo L, Casamassimi A, de Nigris F, Schiano C, Rossiello L, Femiano F, Gombos F,

Napoli C (2008) Evidence of key role of Cdk2 overexpression in pemphigus vulgaris. J Biol Chem 283:8736–8745
Lehman JJ, Kelly DP (2002) Transcriptional activation of energy metabolic switches in the developing and hypertrophied heart. Clin Exp Pharmacol Physiol 29:339–345
Leu M, Ehler E, Perriard JC (2001) Characterisation of postnatal growth of the murine heart. Anat Embryol (Berl) 204:217–224
Matzinger P (1994) Tolerance, danger, and the extended family. Annu Rev Immunol 12:991–1045
Mavroidis M, Capetanaki Y (2002) Extensive induction of important mediators of fibrosis and dystrophic calcification in desmin-deficient cardiomyopathy. Am J Pathol 160:943–952
McDowell EM, Trump BF (1976) Histologic fixatives suitable for diagnostic light and electron microscopy. Arch Pathol Lab Med 100:405–414
Milner DJ, Mavroidis M, Weisleder N, Capetanaki Y (2000) Desmin cytoskeleton linked to muscle mitochondrial distribution and respiratory function. J Cell Biol 150:1283–1298
Morkin E (2000) Control of cardiac myosin heavy chain gene expression. Microsc Res Tech 50:522–531
Nahrendorf M, Swirski FK, Aikawa E, Stangenberg L, Wurdinger T, Figueiredo JL, Libby P, Weissleder R, Pittet MJ (2007) The healing myocardium sequentially mobilizes two monocyte subsets with divergent and complementary functions. J Exp Med 204:3037–3047
Nakai A, Yamaguchi O, Takeda T, Higuchi Y, Hikoso S, Taniike M, Omiya S, Mizote I, Matsumura Y, Asahi M, Nishida K, Hori M, Mizushima N, Otsu K (2007) The role of autophagy in cardiomyocytes in the basal state and in response to hemodynamic stress. Nat Med 13:619–624
Nishida K, Kyoi S, Yamaguchi O, Sadoshima J, Otsu K (2009) The role of autophagy in the heart. Cell Death Differ 16:31–38
Pieperhoff S, Franke WW (2007) The area composita of adhering junctions connecting heart muscle cells of vertebrates - IV: coalescence and amalgamation of desmosomal and adhaerens junction components - late processes in mammalian heart development. Eur J Cell Biol 86:377–391
Pilichou K, Remme CA, Basso C, Campian ME, Rizzo S, Barnett P, Scicluna BP, Bauce B, van den Hoff MJ, de Bakker JM, Tan HL, Valente M, Nava A, Wilde AA, Moorman AF, Thiene G, Bezzina CR (2009) Myocyte necrosis underlies progressive myocardial dystrophy in mouse dsg2-related arrhythmogenic right ventricular cardiomyopathy. J Exp Med 206:1787–1802
Portbury AL, Willis MS, Patterson C (2011) Tearin' up my heart: proteolysis in the cardiac sarcomere. J Biol Chem 286:9929–9934
Posch MG, Posch MJ, Geier C, Erdmann B, Mueller W, Richter A, Ruppert V, Pankuweit S, Maisch B, Perrot A, Buttgereit J, Dietz R, Haverkamp W, Ozcelik C (2008) A missense variant in desmoglein-2 predisposes to dilated cardiomyopathy. Mol Genet Metab 95:74–80
Psarras S, Mavroidis M, Sanoudou D, Davos CH, Xanthou G, Varela AE, Panoutsakopoulou V, Capetanaki Y (2011) Regulation of adverse remodelling by osteopontin in a genetic heart failure model. Eur Heart J July 20 [Epub ahead of print]
Richardson P, McKenna W, Bristow M, Maisch B, Mautner B, O'Connell J, Olsen E, Thiene G, Goodwin J, Gyarfas I, Martin I, Nordet P (1996) Report of the 1995 World Health Organization/International Society and Federation of Cardiology Task Force on the Definition and Classification of cardiomyopathies. Circulation 93:841–842
Thomason HA, Scothern A, McHarg S, Garrod DR (2010) Desmosomes: adhesive strength and signalling in health and disease. Biochem J 429:419–433
Whelan RS, Kaplinskiy V, Kitsis RN (2010) Cell death in the pathogenesis of heart disease: mechanisms and significance. Annu Rev Physiol 72:19–44
Xu X, Yang D, Ding JH, Wang W, Chu PH, Dalton ND, Wang HY, Bermingham JR Jr, Ye Z, Liu F, Rosenfeld MG, Manley JL, Ross J Jr, Chen J, Xiao RP, Cheng H, Fu XD (2005) ASF/SF2-regulated CaMKIIdelta alternative splicing temporally reprograms excitation-contraction coupling in cardiac muscle. Cell 120:59–72
Zhou YQ, Foster FS, Parkes R, Adamson SL (2003) Developmental changes in left and right ventricular diastolic filling patterns in mice. Am J Physiol Heart Circ Physiol 285:H1563–H1575